Reverse nonequilibrium molecular dynamics simulation of thermal conductivity in nanoconfined polyamide-6,6

ARTICLE *in* THE JOURNAL OF CHEMICAL PHYSICS · AUGUST 2011

Impact Factor: 2.95 · DOI: 10.1063/1.3623471 · Source: PubMed

3 AUTHORS, INCLUDING:

Leila Mohammadzadeh
Universität Ulm
6 PUBLICATIONS **29** CITATIONS
SEE PROFILE

Nargess Mehdipour
Persian Gulf University
18 PUBLICATIONS **104** CITATIONS
SEE PROFILE

Reverse nonequilibrium molecular dynamics simulation of thermal conductivity in nanoconfined polyamide-6,6

Hossein Eslami, Laila Mohammadzadeh, and Nargess Mehdipour

Citation: The Journal of Chemical Physics **135**, 064703 (2011); doi: 10.1063/1.3623471
View online: http://dx.doi.org/10.1063/1.3623471
View Table of Contents: http://scitation.aip.org/content/aip/journal/jcp/135/6?ver=pdfcov
Published by the AIP Publishing

Reverse nonequilibrium molecular dynamics simulation of thermal conductivity in nanoconfined polyamide-6,6

Hossein Eslami,[a] Laila Mohammadzadeh, and Nargess Mehdipour
Department of Chemistry, College of Sciences, Persian Gulf University, Boushehr 75168, Iran

(Received 8 June 2011; accepted 19 July 2011; published online 10 August 2011)

A new molecular dynamics simulation method, with coupling to external baths, is used to perform equilibrium simulations on polyamide-6,6 trimers nanoconfined between graphene surfaces, in equilibrium with the bulk polymer. The method is coupled with the reverse nonequilibrium molecular dynamics simulation technique to exchange heat in the direction normal to the surfaces. To be able to study the effect of confinement on the heat conductance in nanoconfined pores, in this work a number of simulations on systems with different pore sizes are done. It is concluded that the coefficient of heat conductivity depends on the degree of polymer layering between the surfaces and on the pore width. Our results further indicate a considerable temperature drop at the interface between the surfaces and polymer. The calculated Kapitza lengths depend on the intersurface distance and on the layering of the polymer nanoconfined between the surfaces. © *2011 American Institute of Physics*. [doi:10.1063/1.3623471]

I. INTRODUCTION

Due to the shrinking in the size of electronic devices, the use of materials with low dielectric constant, like polymers, in such devices is essential. Ultrathin films of polymers have important applications in the development of micromachined sensors, actuators, logic circuits, optical recording discs, and organic optoelectronic devices. For example, in thermomechanical data storage, a heated atomic force microscopy (AFM) cantilever forms a divot, with radius of curvature below 20 nm, in a polymer film of thickness near 30 nm on a silicon substrate.[1] The bit writing rate, therefore, depends on the nanoscale heat transport in the vicinity of the cantilever. Moreover, for application as active and passive layers in circuitry, a higher thermal conductivity of the polymer film is required, in order to reduce the temperature rise and the temperature gradient, and hence, increase the performance and the lifetime of the organic devices. The unusual optical, electrical, thermal, mechanical, and chemical characteristics of ultrathin films arise from the extremely small dimensions of the film and from their enormous surface area per unit volume. It is thus critically important for device design purposes to understand the influence of nanometer-scale pores on the conduction of heat in thin films.

So far a number of experimental techniques, such as transient electrical heating,[2] nano-second thermoreflectance,[3] scanned probe microscopy,[4] and AFM,[5] have been applied to investigate the heat conduction in micrometric and nanometric films. The experimental difficulties arise from the severely limited capabilities for measuring thermal transport in increasingly small systems. Theoretically, several approaches exist to predict the thin-film thermal conductivity for materials where heat conduction by lattice vibrations, or phonons, is dominant. These approaches include kinetic theory,[6] geometric analysis,[7] and the Boltzmann transport theory-based equation of phonon radiative transfer.[8] Such theories, however, are not appropriate to the case of confined liquid films, due to the decrease in the order compared to the solids.

In fact, the difference between the properties of liquids and the confining solids leads to a thermal resistance, known as Kapitza resistance.[9] Theoretically, the thermal resistance at the solid-liquid interface is explained by taking into account the transmission and reflection of classical heat waves at the interface in the so-called acoustic mismatch, diffuse mismatch, and microscale acoustic impedance mismatch models.[10–12] However, these models do not take into account the explicit interactions between the fluid and the surfaces. On the other hand, there is an increasing demand on the microscopic level understanding of heat and mass transfer in nanometer-scale regimes, due to the recent advances in nanoscale heat transfer and in nanotechnology. At present molecular dynamics (MD) simulation is becoming an efficient tool to investigate microscale and nanoscale heat transfer processes.

Despite the technological importance of thin films in thermally sensitive applications, the reports on the MD simulations of the thermal conductivity of thin films of liquids in contact with solid surfaces are scarce. Early MD simulation studies in this field go back to the works by Maruyama *et al.*[13,14] on the MD simulation of Lennard-Jones (LJ) fluid in contact with LJ surfaces. There exist numerous other MD simulation studies on thermal transport in model LJ liquid in contact with surfaces,[15–24] but simulations of more complex (realistic) fluids in contact with surfaces are very scarce. Recently Murad and Puri[25,26] have conducted MD simulations of heat transfer of water in contact with silica surfaces. In another recent work, Xu and Buehler[27] performed MD simulations to study the heat transfer performance of carbon nanotubes wrapped by polyethylene. However, to our knowledge there exists no report on the thermal conductivity calculation

[a]Author to whom correspondence should be addressed. Electronic mail: h.eslami@theo.chemie.tu-darmstadt.de.

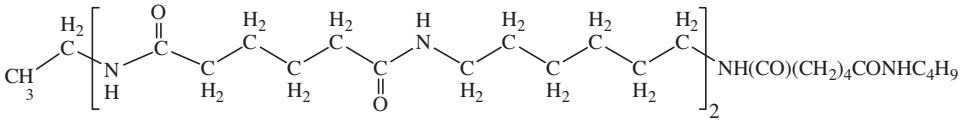

FIG. 1. Chemical structure of a PA-6,6 oligomer studied in this work.

of realistic nanomertic polymer films confined between solid surfaces.

In the case of nanoconfined polymers, even equilibrium MD simulations in the literature are scarce. Most of the equilibrium simulations in the literature are performed for simple LJ fluid confined between LJ surfaces.[28–32] In most of the simulations performed on confined polymer systems, the investigators have used a generic bead-spring model to study, mostly, the equilibrium structure of the confined polymer melts.[33–40] There are a limited number of reports on the detailed MD simulations (atomistic or united atom models) of polymers confined between solid surfaces, most of them focusing on the simulation of polymers with relatively simple chemical structures.[41–43] Another weakness of most of the simulations in the literature is that the fluid in the confined region is not kept in equilibrium with a bulk fluid. This is due to the fact that to keep the fluid in confinement in equilibrium with the bulk fluid, one must either perform the simulation in the grand canonical ensemble,[44,45] or to include the bulk molecules in the simulation box explicitly.[46] Both methods are unfeasible in the case of polymeric systems; the applicability of the former method is hindered due to the impractical insertion/deletion of big polymer molecules into/from the simulation box and in the later method the inclusion of bulk molecules in the simulation box wastes most of the time through simulation of bulk molecules without possibility of exchanging slowly moving polymer molecules between the confined and bulk regions.

Very recently we have developed a simulation scheme for the simulation of fluids in confinement.[47] In fact we have developed the MD simulation method of Berendsen *et al.*,[48] with coupling to an external bath, to simulate the confined fluid at a constant number of confined particles, N, constant surface area, A, constant temperature, T, and constant parallel component of the pressure, $P_\parallel$, which we call *NAPT* ensemble simulation hereafter. It is shown that this method reproduces the results for the grand canonical ensemble simulation of confined LJ fluid[49–51] and the results for water confined between graphite surfaces,[46] in which the water molecules in confinement are in equilibrium with a reservoir of bulk molecules. The method is shown to mimic the surface force apparatus experiment[52,53] and is extended to the case of equilibrium structure[54] and viscosity calculation[55] of nanoconfined PA-6,6. As the extension of our previous works,[54,55] in this work we couple this method with the reverse nonequilibrium molecular dynamics (RNEMD) simulation technique[56–58] to simulate the heat transport in nanoconfined PA-6,6 films.

II. METHOD

In this work, equilibrium MD simulations are performed in the *NAPT* ensemble.[47] The details of the simulation method are described elsewhere.[47] Here we restrict ourselves to the description of some basic elements of the method. Here the system, including the polymer in confinement as well as the confining surfaces, is coupled to a heat bath at a fixed temperature by scaling the velocities at each time step according to the method of Berendsen *et al.*[48] The system is further coupled to a barostat by keeping the parallel component of the pressure, $P_\parallel$, fixed. The parallel component of the pressure is defined as follows:[47]

$$P_{||} = \frac{P_{xx} + P_{yy}}{2} = \frac{1}{3V}\sum_i m_i v_i^2 + \frac{1}{2V} \times \left[\sum_i \sum_{j>i} (X_{ij}.F_{x,ij} + Y_{ij}.F_{y,ij}) + \sum_i \sum_k (X_{ik}.F_{x,ik} + Y_{ik}.F_{y,ik}) \right] + \frac{1}{2V}\left[\sum_k \sum_{l>k} (X_{kl}.F_{x,kl} + Y_{kl}.F_{y,kl}) \right], \quad (1)$$

where P_{xx} and P_{yy} are the x- and y-components of pressure tensor, respectively, m is the atomic mass, V is the volume, subscripts i and j show the atoms in the confined region, subscripts k and l stand for the surface atoms, $\boldsymbol{X}$ and $\boldsymbol{Y}$ are the relative distances between particles in the x and y directions, respectively, and $\boldsymbol{F}_x$ and $\boldsymbol{F}_y$ are their corresponding forces. We have shown[47] that this coupling amounts to scaling the z-coordinates of all particles per time step from z to μz with

$$\mu = 1 - \beta \Delta t \frac{(P_{0,||} - P_{||})}{\tau_P}. \quad (2)$$

In Eq. (2), β is the isothermal compressibility, $P_{0,\parallel}$ is the target value of the parallel component of pressure, and τ_P is the time constant for pressure coupling, determining the strength of coupling to the barostat. Therefore, in this method the distance between the surfaces, h, is changed dynamically to keep $P_\parallel$ fixed.

Employing the *NAPT* ensemble simulation method,[47] an initially relaxed configuration of PA-6,6 oligomers, confined between graphene surfaces, is generated to start the RNEMD simulations. The chemical structure of a PA-6,6 oligomer is shown in Fig. 1. In the RNEMD method,[56–58] unlike what is done in experiment, (heat) flux is imposed and the corresponding force is measured. The force and flux are related together via the linear response theory, i.e.,

$$J_z = -\lambda \frac{dT}{dz}, \quad (3)$$

where J_z is the heat flux in the z direction, dT/dz is the temperature gradient along the z direction (force), and λ is the coefficient of thermal conductivity. The heat flux is defined

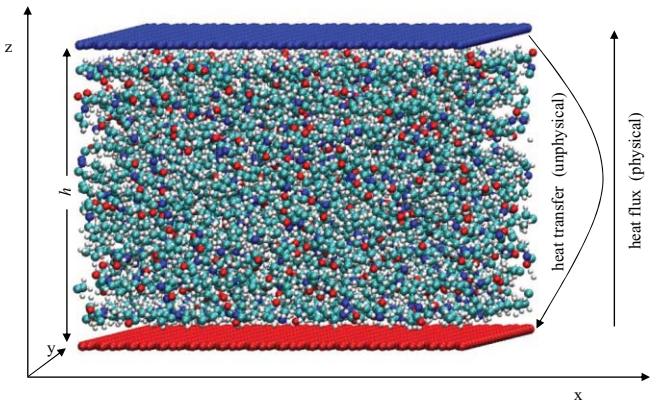

FIG. 2. Snapshot of a simulation box with PA-6,6 oligomers confined between graphene surfaces. The arrows indicate the imposed (unphysical) and the physical heat fluxes between hot (red) and cold (blue) surfaces.

as the amount of heat transferred per unit time per unit area of a surface perpendicular to the direction of heat flow. To perform the unphysical heat transfer we do as follows: The simulation box, which is periodic in the x and y directions but not in the z direction, is divided into several slabs along the z direction. Here one of the graphene surfaces, located at $z = -h/2$, is regarded as the first slab and the other one, located at $z = h/2$, is the last slab. A snapshot of the simulation box as well as the coordinate system is given in Fig. 2. The coldest atom (the atom with the smallest kinetic energy) in the first (hot) slab is found. Similarly, in the last (cold) slab the hottest atom (the atom with the largest kinetic energy) is found. Then all the Cartesian components of the velocities of these two atoms are exchanged. Here the surface atoms all have the same mass, therefore the unphysical heat exchange conserves the kinetic energy of the system as a whole; since the position of the atoms are not changed, the potential energy and hence the total energy of the system is conserved. In the steady state the average heat transferred from the cold to hot slab is calculated as

$$J_z = \frac{1}{At} \sum_{\text{transferes}} \frac{m}{2} \left(v_{\text{hot}}^2 - v_{\text{cold}}^2 \right), \tag{4}$$

where A is the surface area, t is the simulation time, and subscripts hot and cold refer to the hot and the cold slabs, respectively. In this work, this method is employed to study the nanometer-scale heat flow in PA-6,6 confined between graphene surfaces.

III. SIMULATION DETAILS

Atomistic MD simulations were performed for ethyl- and butyl-terminated PA-6,6 trimers, containing 6 amide groups (see Fig. 1). The oligomers of PA-6,6 studied in this work may seem too short to be representatives of realistic PA-6, 6 chains. However one should keep in mind that choosing a longer PA-6,6 chain may cause the freezing of the polymer in the pore. Meanwhile, it is worth considering that each PA-6,6 trimer, studied in this work, contains 116 atoms, which is shown to be long enough to represent many characteristics of a realistic PA-6,6 chain.[54,55] To be able to study the effect of pore size and oligomer conformation on the thermal conductivity, totally seven systems (six confined systems with various ratios of the surface area to the intersurface distance as well as a bulk system) are simulated in this work. The details of the systems simulated are given in Table I. At the first stage, equilibrium MD simulations were performed in the *NAPT* ensemble[47] at $T = 400$ K and $P_{\parallel} = 101.3$ kPa. The atomistic force-field parameters for PA-6,6 oligomers as well those of confining graphene surfaces are given in Ref. 54. The parameters for unlike interactions were determined using Lorentz-Berthelot mixing rules.[59] All MD simulations were carried out using the simulation package, YASP.[60,61] All nonbonded interactions were truncated at 0.95 nm with a reaction field correction for the Coulombic interactions.[59] The effective dielectric constant was taken to be 5.5.[54,62] An atomic Verlet neighbor list was used, which was updated every 15 time steps, and the neighbors were included if they were closer than 1.0 nm. The time step was 1.0 fs. Preparing initially relaxed configurations of the nanoconfined systems, tabulated in Table I, we performed RNEMD simulations, employing the method outlined in Sec. II. The simulation box was divided to a proper number of slabs and heat exchange between the cold and hot slabs was done by repeatedly exchanging the kinetic energies, as explained above.

TABLE I. Description of systems simulated in this work.[a]

System	Number of oligomers	N_g	N	A (nm^2)	$\langle h \rangle$ (nm)
S_1	75	4300	17 300	112.633	0.9931
S_2	75	2232	13 164	58.465	1.7932
S_3	100	1972	15 544	51.654	2.3888
S_4	100	1500	14 600	39.291	3.2027
S_5	125	1500	17 500	39.291	3.8417
S_6	150	1144	19 688	29.966	5.9354
S_7 (bulk)	250		29 000		

[a]N_g, N, A, and $\langle h \rangle$ are the number of C atoms per each graphene sheet, the total number of atoms, surface area (of one surface), and the average intersurface separation, respectively.

IV. RESULTS AND DISCUSSION

A. Local density profiles and solvation force oscillations

It is well known that fluids confined in nanometric pores from well formed structures beside the surfaces.[47] Here we have shown the distribution of the mass density of confined systems studied in this work in Fig. 3. Dividing the distance between the surfaces into a number of tiny slabs and averaging the mass density of atoms in each slab during the equilibrium MD simulations in the *NAPT* ensemble,[47] the results in Fig. 3 show that PA-6,6 oligomers form layered structures near the surfaces. The degree of layering and the number of peaks depend on the intersurface separations. We have also calculated the average solvation force; the average force exerted by the confined film on the confining surfaces, $\langle f_s \rangle$, and showed the results in Fig. 4. The results show that on formation of well organized layers between the surfaces, the

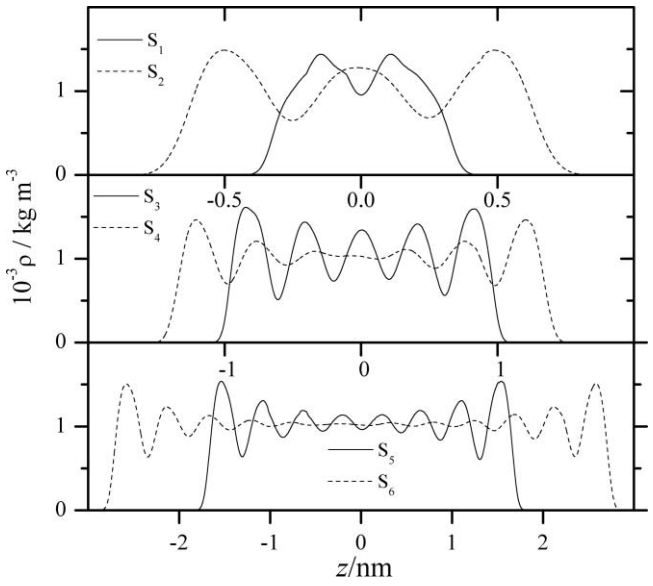

FIG. 3. Local density profiles for systems S_1-S_6 at $T = 400$ K and $P_{\parallel} = 101.3$ kPa. The number of oligomers, surface areas, and average surface separations are given in Table I.

solvation force shows maxima. Controversially, the positions of minima in the solvation force curve correspond to the formation of diffuse layers between the surfaces. This can be revealed by comparing Figs. 3 and 4 for systems S_1 and S_3, with positive solvation forces, and system S_2, with a negative solvation force.

B. Linear temperature profiles

Having divided the box length in the z direction into a proper number of slabs, unphysical heat flow is imposed between the surfaces by exchanging the kinetic energies of C atoms of the surfaces. A snapshot of the simulation box is given in Fig. 2, in which the coldest and the hottest slabs (surfaces) are indicated in blue and red, respectively. As a result of imposing such an unphysical heat flux in the system,

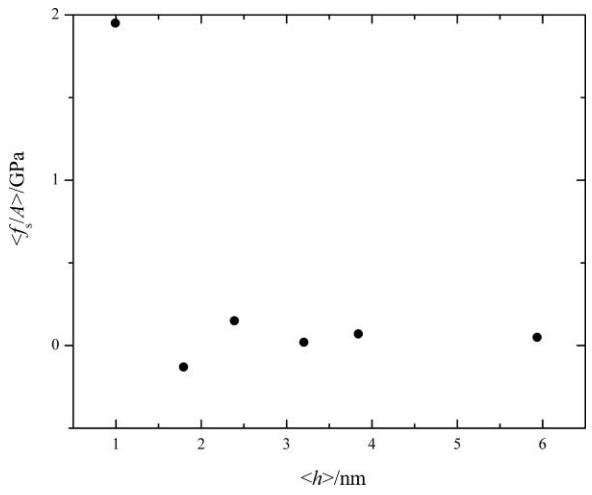

FIG. 4. Calculated average solvation force as a function of average surface separation at $T = 400$ K and $P_{\parallel} = 101.3$ kPa.

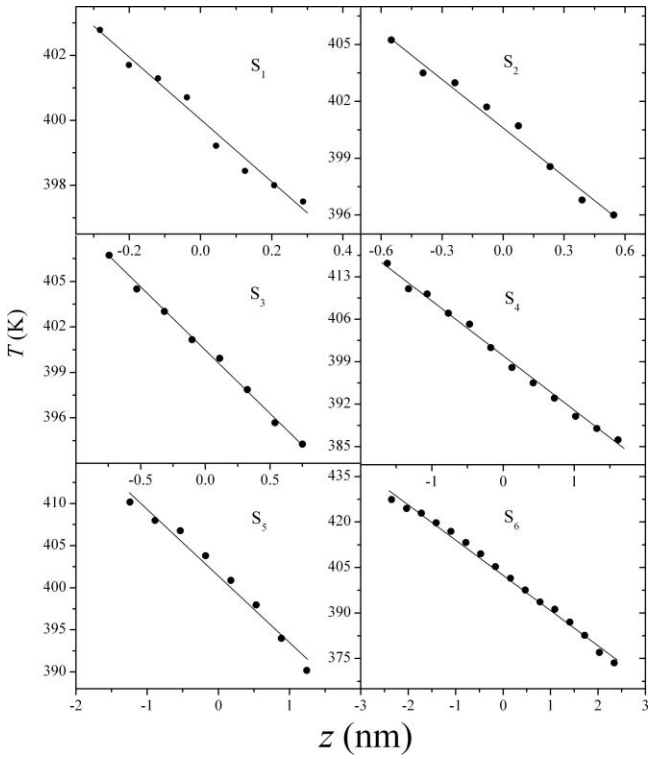

FIG. 5. Linear temperature profiles for heat flow in systems S_1-S_6. The average temperature of the whole system (polymer+surfaces) is 400 K and $P_{\parallel} = 101.3$ kPa. The lines indicate the best linear fit through the points. Except for system S_1, for which the exchange period is 100 ns, for rest of the systems the exchange period is 300 ns.

the heat transfer occurs in the system in the opposite direction (see Fig. 2). At the steady state a linear temperature profile will be developed in the pore in the direction of heat flow. We have performed RNEMD calculations for a time span of 5.0 ns to achieve the steady state. Another 5 ns of RNEMD simulations were performed for the sake of data collection. The linear temperature profiles for systems S_1-S_6 are given in Fig. 5. It is worth considering that in Fig. 5 only the temperature profiles inside the pore (polymer) are given and the temperatures of surfaces are excluded form the profiles. In Sec. IV C we turn back to this point.

In the linear-response regime, as Eq. (3) indicates, the coefficient of thermal conductivity must be independent of the magnitude of the imposed flux (exchange period). The validity of linear response theory has been checked in all RNEMD simulations in this work. We have shown in Fig. 6 the linear temperature profiles at different exchange periods for system S_1, as a typical example. The results show that linear temperature profiles develop in the pore over a wide range of imposed fluxes.

Within the applicability of linear response theory, adopting a smaller exchange period (imposing a higher heat flux) develops the steady state in a shorter time. Imposing lower heat fluxes (smaller exchange frequencies) assures the validity of the linear response theory, but longer simulations are needed to achieve the steady state. Although the results in Fig. 6 indicate the validity of the linear response theory over a wide range of exchange periods, in this work we have tried to choose low enough exchange periods to be sure that the

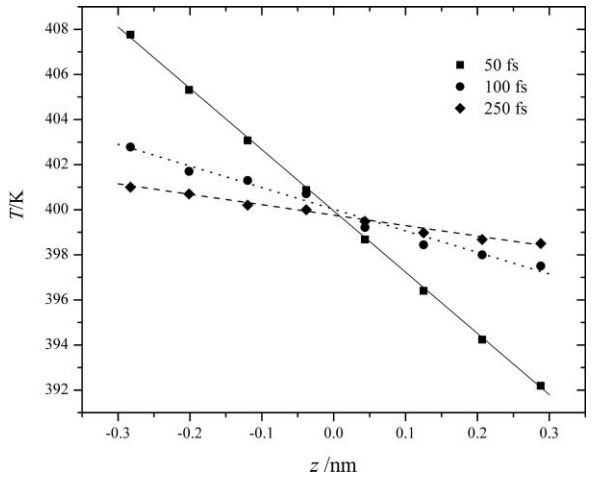

FIG. 6. Linear temperature profiles for heat transfer in system S_1 at different exchange periods, shown in the figure.

response of the system to the imposed heat flux is linear. The force, dT/dz in Eq. (3) can easily be calculated from the slope of such a linear temperature profile.

To be able to compare the results for heat transfer in confined polymer with those of bulk sample, we have also performed RNEMD simulations for a bulk sample (S_7) of PA-6,6 at $T = 400$ K and $P = 101.3$ kPa. In this case, to increase the statistics, the simulation box is elongated in the direction of heat flow (z direction). The result for a linear temperature profile in the bulk polymer is shown in Fig. 7.

C. Kapitza distance

As early as 1941 Kapitza[9] noticed the phenomenon of thermal resistance at the interface between copper and liquid helium. Later it was realized that such an interfacial thermal resistance, Kaptiza resistance, exists at the interface between any pair of dissimilar materials. Therefore due to this phenomenon, a temperature drop is observed at the interfaces. In

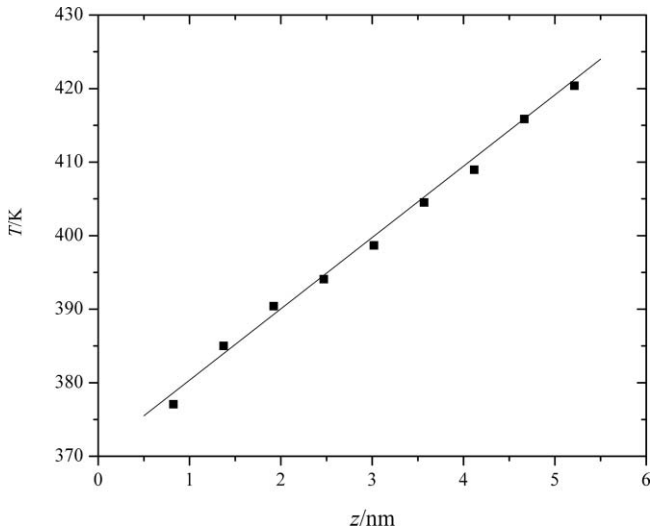

FIG. 7. The same as Fig. 5, but for the bulk PA-6,6 sample. The exchange period is 300 fs.

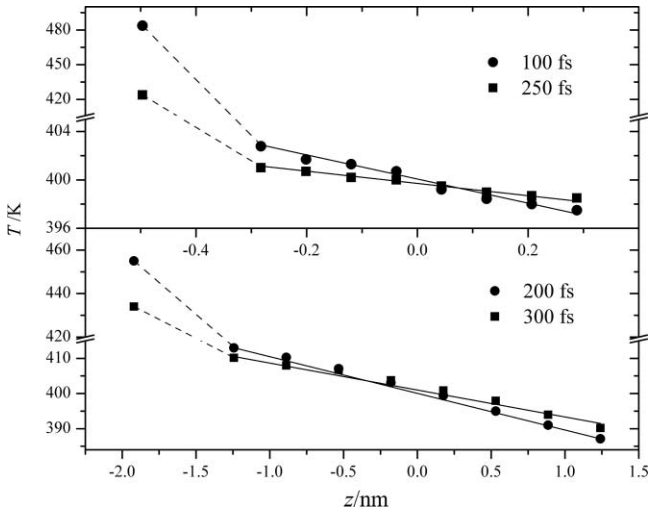

FIG. 8. Temperature drop between the surfaces and polymer in confinement for systems S_1 (top panel) and S_5 (bottom panel). The exchange periods are shown in the figure. The solid lines indicate the best linear fit through the individual temperature points in the pore and the dashed lines connect the temperature of the surface to that of the polymer slab in its vicinity.

Fig. 8 we have shown the temperature profiles for systems S_1 and S_5, as typical examples, at different exchange periods. For the sake of simplicity, the temperature of just one of the surfaces is shown in the figure. As it can be seen from the results, a large temperature drop is observed at the interface between the graphene surfaces and the polymer. Moreover, the magnitude of the temperature drop at the solid-liquid interface depends on the magnitude of the imposed heat flux and on the pore size.

To understand the significance of the Kapitza resistance in nanoconfined geometries, one can express it in terms of the thermal resistance thickness, called the Kapitza length, l_K. The Kaptiza length can be obtained by extrapolating the temperature profile from the confined fluid to the confining surface, where the surface temperature is reached. The Kapitza length is therefore expressed as

$$l_K = \frac{T_s - T_f}{dT/dz}, \tag{5}$$

where T_s and T_f are the temperatures of the surface and the fluid, respectively, and dT/dz is the slope of the linear temperature profile in the fluid. In Fig. 9 we have shown the Kapitza length as a function of pore width at a fixed exchange period. The results show that the Kapitza length depends on the pore width. The Kapitza length also shows an oscillatory behavior with respect to the pore width, similar to the oscillations in solvation force curve.

D. Thermal conductivities

As it is explained in Sec. II, in this method the amount of flux (imposed) is exactly known. Therefore, having obtained linear temperature profiles, such as those reported in Figs. 5–7, one can calculate the coefficient of thermal conductivity employing Eq. (3). In Fig. 10 we have shown the calculated thermal conductivities. For the sake of comparison, the thermal conductivity of the bulk sample of PA-6,6 is also given

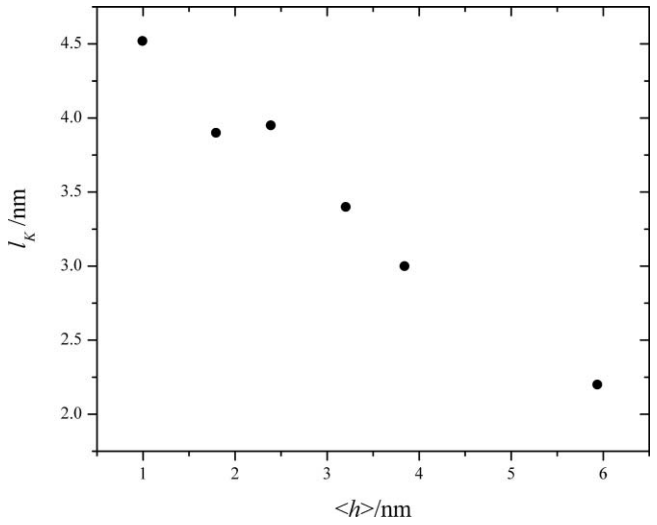

FIG. 9. The Kapitza length, l_K, for systems S_1-S_6 at an exchange period of 300 ns as a function of average surface separation.

in the same figure. The results show that the calculated thermal conductivity coefficients depend on the pore width. On the other hand, strong deviations in the thermal conductivities, with respect to that of bulk PA-6,6, is seen in very narrow pores. With increasing the distance between the surfaces, the thermal conductivity tends to the thermal conductivity of the bulk fluid. Moreover, the calculated thermal conductivities show oscillatory behavior versus pore width, like the oscillations in the solvation force curve. The results in Fig. 10, therefore, show that the thermal conductivities are related to the degree of layering of PA-6,6 beside the surfaces; well-formed layers with positive solvation forces show higher thermal conductivities.

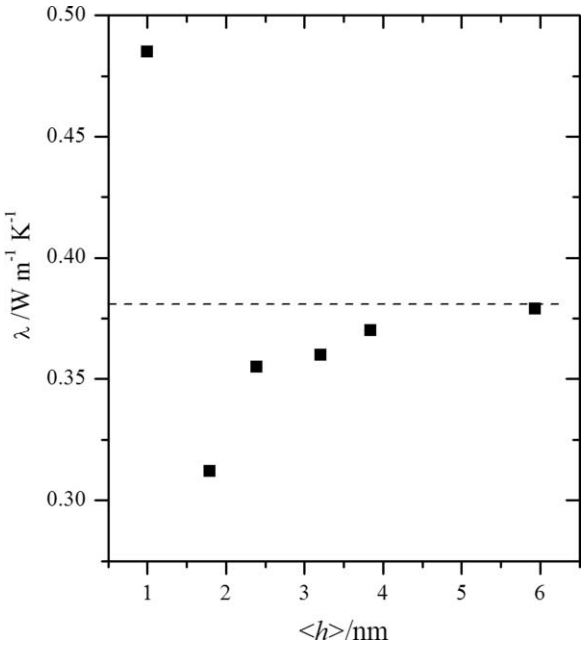

FIG. 10. The calculated coefficients of thermal conductivity as a function of pore width. The dashed line indicates the coefficient of thermal conductivity for the bulk sample.

V. CONCLUSIONS

Our new molecular dynamics simulation method in the *NAPT* ensemble[47] is coupled with the RNEMD simulation technique[56–58] to study the heat conduction in nanoconfined PA-6,6 oligomers. Artificial heat fluxes are imposed in perpendicular direction with respect to the confining graphene surfaces. Our results show that the coefficient of thermal conductivity depends on the intersurface separation and on the degree of layering of oligomers in the pore. Well-organized layers with maxima in the solvation force curve correspond to maxima in the coefficient of heat conduction. The heat flow in the pore, therefore, depends on the pore width and on the layering of polymer in the pore. In well formed layers, a better packing of polymer chains occurs (compared to the diffuse layers). Therefore, better organized layers conduct heat more easily through collisions. Our results further indicate that there is a substantial temperature drop at the interface, which its magnitude depends on the imposed heat flux and on the pore width. Analysis of the Kapitza length in the confined polymer indicates that the Kapitza length also depends on the intersurface separation and on the layering of polymer between the surfaces.

ACKNOWLEDGMENTS

The support of this work by the Research Committee of Persian Gulf University is gratefully acknowledged. The authors would like to thank Mr. Mohammad Rahimi for the helpful discussions during preparation of the manuscript.

[1]D. G. Cahill, W. K. Ford, K. E. Goodson, G. D. Mahan, A. Majumdar, H. J. Maris, R. Merlin, and S. R. Phillpot, J. Appl. Phys. **93**, 703 (2003).
[2]K. Kurabayashi, M. Asheghi, M. Touzelbaev, and K. E. Goodson, IEEE J. Micromech. Sys. **8**, 180 (1999).
[3]M. Kuwahara, O. Suzuki, S. Takada, N. Hata, P. Fons, and J. Tominaga, Microelectron. Eng. **85**, 796 (2008).
[4]A. Hammiche, M. Reading, H. M. Pollock, M. Song, and D. J. Hourston, Rev. Sci. Instrum. **67**, 4268 (1996).
[5]W. P. King, T. W. Kenny, K. E. Goodson, G. Cross, M. Despont, U. Durig, H. Rothuizen, G. K. Binnig, and P. Vettiger, Appl. Phys. Lett. **78**, 1300 (2001).
[6]J. M. Ziman, *Electrons and Phonons* (Oxford University Press, London, 1960).
[7]M. I. Flik and C. L. Tien, J. Heat Transfer **112**, 872 (1990).
[8]A. Majumdar, J. Heat Transfer **115**, 7 (1993).
[9]P. L. Kapitza, Zh. Eksp. Theor. Fiz. **11**, 1 (1941).
[10]W. A. Little, Can. J. Phys. **37**, 334 (1959).
[11]E. T. Schwartz and R. O. Pohl, Rev. Mod. Phys. **61**, 605 (1989).
[12]S.-H. Choi, S. Maruyama, K. K. Kim, and J. H. Lee, J. Korean Phys. Soc. **44**, 317 (2004).
[13]S. Maruyama, T. Kurashige, S. Matsumoto, Y. Yamaguchi, and T. Kimura, Microscale Thermophys. Eng. **2**, 49 (1998).
[14]S. Maruyama and T. Kimura, Therm. Sci. Eng. **7**, 63 (1999).
[15]L. Xue, P. Keblinski, S. R. Phillpot, S. U. Choi, and J. A. Eastman, Int. J. Heat Mass Transfer **47**, 4277 (2004).
[16]R. Khare, P. Keblinski, and A. Yethiraj, Int. J. Heat Mass Transfer **49**, 3401 (2006).
[17]C. S. Wang, J. S. Chen, J. Shiomi, and S. Maruyama, Int. J. Therm. Sci. **46**, 1203 (2007).
[18]C. F. Carlborg, J. Shiomi, and S. Maruyama, Phys. Rev. B **78**, 2054061 (2008).
[19]G. Balasubramanian, S. Banerjee, and I. K. Puri, J. Appl. Phys. **104**, 064306 (2008).
[20]B. H. Kim, A. Beskok, and T. Cagin, J. Chem. Phys. **129**, 174701 (2008).
[21]J. Sun, Y-L. He, and W-Q. Tao, Int. J. Meth. Engng. **81**, 207 (2010).
[22]S. C. Maroo and J. N. Chung, J. Nanopart. Res. **12**, 1913 (2010).

[23]D. Torii, T. Ohara, and K. Ishida, J. Heat Transfer **132**, 012402 (2010).
[24]S. Wang and X. Liang, Int. J. Thermophys. **31**, 1935 (2010).
[25]S. Murad and I. K. Puri, Chem. Phys. Lett. **467**, 110 (2008).
[26]S. Murad and I. K. Puri, Appl. Phys. Lett. **92**, 133105 (2008).
[27]Z. Xu and M. J. Buehler, ACS Nano **3**, 2767 (2009).
[28]M. Schoen, C. L. Rhykerd, D. J. Diestler, and J. H. Cushman, Science **245**, 1223 (1989).
[29]M. Schoen, D. J. Diestler, and J. H. Cushman, J. Chem. Phys. **100**, 7707 (1994).
[30]B. D. Todd, D. J. Evans, and P. J. Daivis, Phys. Rev. E **52**, 1627 (1995).
[31]J. Gao, W. D. Luedtke, and U. Landman, Phys. Rev. Lett. **79**, 705 (1997).
[32]J. C. Wang and K. A. Fichthorn, J. Chem. Phys. **112**, 8252 (2000).
[33]K. F. Mansfield and D. N. Theodorou, Macromolecules **22**, 3143 (1989).
[34]A. Yethiraj and C. K. Hall, Macromolecules **23**, 1865 (1990).
[35]A. Yethiraj, J. Chem. Phys. **101**, 2489 (1994).
[36]J. Gao, W. D. Luedtke, and U. Landman, J. Phys. Chem. B **101**, 4013 (1997).
[37]S. T. Cui, P. T. Cummings, and H. D. Cochran, J. Chem. Phys. **114**, 7189 (2001).
[38]J. H. Jeon, S. H. Kim, and W. H. Jo, Macromol. Theory Simul. **11**, 147 (2002).
[39]S. T. Cui, C. McCabe, and P. T. Cummings, J. Chem. Phys. **118**, 8941 (2003).
[40]Y. Leng and P. T. Cummings, Phys. Rev. Lett. **94**, 026101 (2005).
[41]O. Borodin, G. D. Smith, R. Bandyopadhyaya, and O. Byutner, Macromolecules **36**, 7873 (2003).
[42]K. Ch. Daoulas, V. A. Harmandaris, and V. G. Mavrantzas, Macromolecules **38**, 5780 (2005).
[43]V. A. Harmandaris, K. Ch. Daoulas, and V. G. Mavrantzas, Macromolecules **38**, 5796 (2005).
[44]H. Eslami and F. Müller-Plathe, J. Comput. Chem. **28**, 1763 (2007).
[45]H. Eslami, F. Mojahedi, and J. Moghadasi, J. Chem. Phys. **133**, 084105 (2010).
[46]N. Choudhury and B. M. Pettitt, J. Am. Chem. Soc. **127**, 3556 (2005).
[47]H. Eslami, F. Mozaffari, J. Moghadasi, and F. Müller-Plathe, J. Chem.Phys. **129**, 94702 (2008).
[48]H. J. C. Berendsen, J. P. M. Postma, W. F. van Gunsteren, A. DiNola, and J. R. Haak, J. Chem. Phys. **81**, 3684 (1984).
[49]M. Schoen, D. J. Diestler, and J. H. Cushman, J. Chem. Phys. **87**, 5464 (1987).
[50]M. Schoen, D. J. Diestler, and J. H. Cushman, J. Chem. Phys. **100**, 7707 (1994).
[51]M. Schoen, D. J. Diestler, and J. H. Cushman, Phys. Rev. B **47**, 5603 (1993).
[52]B. Bhushan, J. N. Israelachvili, and U. Landman, Nature (London) **374**, 607 (1995).
[53]J. N. Israelachvili, P. M. McGuiggan, and A. M. Homola, Science **240**, 189 (1988).
[54]H. Eslami and F. Müller-Plathe, J. Phys. Chem. B **113**, 5568 (2009).
[55]H. Eslami and F. Müller-Plathe, J. Phys. Chem. B **114**, 387 (2010).
[56]F. Müller-Plathe, Phys. Rev. E. **59**, 4894 (1999).
[57]F. Müller-Plathe and D. Reith, Comput. Theor. Polym. Sci. **9**, 203 (1999).
[58]P. Bordat and F. Müller-Plathe, J. Chem. Phys. **116**, 3362 (2002).
[59]M. P. Allen and D. J. Tildesley, *Computer Simulation of Liquids* (Clarendon Press, Oxford, 1987).
[60]F. Müller-Plathe, Comput. Phys. Commun. **78**, 77 (1993).
[61]K. Tarmyshov and F. Müller-Plathe, J. Chem. Inf. Model. **45**, 1943 (2005).
[62]S. Goudeau, M. Charlot, C. Vergelati, and F. Müller-Plathe, Macromolecules **37**, 8072 (2004).